

## GIANT IMPACTS ON EARTH-LIKE WORLDS

ELISA V. QUINTANA<sup>1,2</sup>, THOMAS BARCLAY<sup>1,3</sup>, WILLIAM BORUCKI<sup>1</sup>, JASON F. ROWE<sup>1,4</sup> AND JOHN E. CHAMBERS<sup>5</sup>

## ABSTRACT

The late stages of terrestrial planet formation are dominated by giant impacts that collectively influence the growth, dynamical stability, composition and habitability of any planets that form. Hitherto, numerical models designed to explore these late stage collisions have been limited in two major ways. First, nearly all  $N$ -body models have assumed that two-body collisions lead to perfect accretion. Second, many of these studies lack the large number of realizations needed to account for the chaotic nature of these  $N$ -body systems. In this article we improve on both of these limitations by performing hundreds of simulations of late stage terrestrial planet formation using an  $N$ -body algorithm that has recently been modified to include fragmentation and hit-and-run collisions. We performed 140 simulations of planet accretion around a Sun-like star with Jupiter and Saturn analogs using this new collision model, and 140 simulations using the standard perfect-accretion model. We find that when fragmentation is included, the final planets formed are similar to those formed in the perfect-accretion model in terms of mass and number, however the paths towards building these planets are significantly different. In fact, neglecting fragmentation leads to an underestimation of the time taken to accrete or eject planetesimals from the system. Over 90% of the fragmentation simulations produced an Earth-analog and we parameterized the impacts onto these planets in terms of their specific impact energies. Only 15 of our 164 Earth-analogs experienced an impact that was energetic enough to strip an entire atmosphere. To strip about half of an atmosphere requires energies comparable to the Moon-forming giant impact, and almost all Earth-analogs received at least one impact that met this criteria and received on average 3.0 of these giant impacts during the 2 Gyr simulations. The median time of the *final* giant impact was 43 Myr after the start of the simulations, leading us to conclude that the time-frame of the Moon-forming impact is typical amongst planetary systems around Sun-like stars.

*Subject headings:* Planetary systems; planets and satellites: formation; methods: data analysis; methods: numerical; planets and satellites: dynamical evolution and stability; planets and satellites: terrestrial planets

## 1. INTRODUCTION

The final stages of terrestrial planet formation are characterized by a myriad of gravity-dominated collisions among bodies in a protoplanetary disk. These impacts can lead to a wide range of outcomes depending on the masses, impact speed, impact angle, composition and number of bodies involved. Taken together, collisions can largely influence a planet's growth, stability, bulk composition and habitability.

Gravitational  $N$ -body algorithms have been widely used for decades to numerically model the late stages of terrestrial planet formation. Numerical integrations of these late stages - in which planets form via pairwise accretion from bodies in a protoplanetary disk - face several major complexities. First,  $N$ -body simulations that include interparticle self gravity are computationally intensive, and the computation time scales as the square of the number of bodies ( $N^2$ ). This is one reason why nearly all previous  $N$ -body models have assumed perfect accretion (meaning two bodies that collide will stick together and conserve mass and momentum), limiting the

maximum  $N$  to the initial number of bodies in the protoplanetary disk. Collisional fragmentation, however, can increase  $N$  so has been neglected in these models. Secondly,  $N$ -body systems with  $N > 2$  are chaotic and thus a large number of simulations of a given system, with very small changes in the initial conditions, are required in order to gain meaningful statistical results.

Despite these limitations, numerical  $N$ -body simulations that assumed perfect accretion have been successful at reproducing the broad characteristics of the terrestrial planets in our Solar System (Wetherill 1994; Chambers 2001; Raymond et al. 2004, 2006; O'Brien et al. 2006; Raymond et al. 2009; Quintana et al. 2002; Quintana & Lissauer 2006, 2010, 2014). These results were all based on a small (up to a dozen) number of realizations performed for each set of initial conditions. A larger set of 50 simulations of planet formation around the Sun was recently performed by Fischer & Ciesla (2014) which, using the perfect-accretion model, demonstrated the need for a larger suite of simulations in order to infer results from a distribution of final planet configurations.

Several recent developments have opened the door to more sophisticated  $N$ -body simulations of late-stage planet formation. Leinhardt & Stewart (2012) and Stewart & Leinhardt (2012) developed a state-of-the-art collisions model for gravity-dominated bodies that essentially maps collision outcomes based on the masses, collision speed and impact angle for a given two-body collision.

<sup>1</sup> NASA Ames Research Center, Moffett Field, CA 94035

<sup>2</sup> NASA NPP Senior Fellow

<sup>3</sup> Bay Area Environmental Research Institute, 625 2nd St. Ste 209, Petaluma, CA 94952

<sup>4</sup> SETI Institute, 189 Bernardo Ave, Mountain View, CA 94043

<sup>5</sup> Department of Terrestrial Magnetism, Carnegie Institution for Science, 5241 Broad Branch Road NW, Washington, DC 20015, United States

This collision model has been implemented into an  $N$ -body tree code (Bonsor et al. 2015; Lines et al. 2014) and used to examine planetesimal formation.

Chambers (2013) implemented this collision model into the widely-used *Mercury* integration package (Chambers 2001). Eight simulations of planet formation around the Sun using this new model were presented and compared to eight simulations that were previously performed using the standard perfect-accretion version of *Mercury*. The final planets that formed in each of these sets were shown to be comparable despite the significant difference in the number and frequency of collisions. In addition, the accretion timescales were about twice as long when fragmentation was included.

Quintana & Lissauer (2014) recently examined planet growth around the Sun with Jupiter and Saturn perturbing the system using the perfect-accretion version of *Mercury*. In this study, a disk model based on Chambers (2001) was used but the disk was extrapolated from 2 AU to 4 AU from the Sun. From 2 – 4 terrestrial planets formed within  $\sim 200$  Myr in each of the six simulations performed. In this article we expand on this work and perform simulations using the same initial conditions for the Sun-Jupiter-Saturn system as Quintana & Lissauer (2014), but we now use the modified version of *Mercury* that allows fragmentation. We have performed an order-of-magnitude larger number of simulations than Quintana & Lissauer (2014) and Chambers (2013). Specifically, 140 simulations using the new fragmentation model and 140 using the perfect-accretion model were performed. This large set of simulations allows us to examine the effects of fragmentation in  $N$ -body models while accounting for the chaotic nature of these systems, thereby improving upon the two main challenges of  $N$ -body planet formation models.

The results from our 280 simulations are presented here. In order to place our simulations in context with the Earth’s history, we first present a chronology of Solar System formation in Section 2. Our numerical model and initial conditions are given in Section 3. In Section 4 we present results on the effects of fragmentation. We then focus on the Earth-analogs that form and examine the giant impacts onto these planets in Section 5, and a summary and conclusions are given in Section 6

## 2. CHRONOLOGY

An approximate timeline that places our  $N$ -body simulations of late stage accretion in context with some of the significant events in the Earth’s history is shown in Figure 1. The beginning of the Solar System’s formation is often defined as the time that the first solids condensed in the Sun’s protoplanetary disk as it cooled. The oldest known substances are Calcium Aluminum Inclusions (CAIs) found in carbonaceous chondrite meteorites, and radiometric dating places their origins at  $\sim 4.567$  billion years ago (Connelly et al. 2012; MacPherson 2014).

Planets then grow by a pair-wise accretion process from a protoplanetary disk of gas and dust that is a remnant of the star’s formation (Safronov & Zvjagina 1969; Lissauer 1993). The early stages of planet formation, from dust to km-sized objects, remain poorly understood, but theories suggest that growth may occur via a gravitational sticking process (Weidenschilling 1977; Krijt et al. 2015) or by gravitational instabilities

(Goldreich & Ward 1973) to create km-sized planetesimals. In the next stage, a runaway growth phase occurs where the largest bodies accrete material faster than smaller bodies until they are large and massive enough for orbital repulsion to take over (Kokubo & Ida 2000). An oligarchic growth phase then takes place, yielding a disk with approximately Mars-sized objects embedded in a swarm of Moon-sized and smaller bodies (Kokubo & Ida 1998).

Geochemical evidence from Martian meteorites provides constraints on the formation timescale of Mars. In turn, these constraints can be used as a proxy for the formation timescale of Mars-sized planetary embryos given that Mars is thought to be essentially a planetary embryo that escaped a significant amount of accretion or erosion during the final stages of planet formation (Dauphas & Pourmand 2011). Isotopic evidence suggests that Mars grew to half its size within about 1.2 – 2 Myr and was mostly formed (accreting  $\sim 90\%$  of its mass) within about 5 Myr (Dauphas & Pourmand 2011; Tang & Dauphas 2014). This would place constraints on the formation of Mars-sized embryos in the protoplanetary disk to within about 5 Myr from the start of Solar System formation. The lifetime of the gas component in the disk is thought to have been  $\sim 3$  – 7 Myr (Haisch et al. 2001; Hernandez et al. 2007, 2010), during which the gas giant planets like Jupiter and Saturn must have formed in order to accrete their gaseous envelopes (Lissauer 1987; Lissauer et al. 2009). Our simulations begin at the epoch at which gas has been dispersed from the disk, the giant planets have formed, and Mars-sized embryos and smaller planetesimals remain and are subject to purely gravitational (no gas drag) perturbations and collisions.

Isotopic constraints and dynamical simulations place the subsequent formation of the Earth somewhere between 30 – 100 Myr after the birth of the Solar System (Chambers 2001; Morbidelli et al. 2012). The Moon is thought to have formed via a giant impact of a large body with the proto-Earth, although the scenario and time of this impact is still under debate. Several different theories have been developed to explain the characteristics of the current Earth-Moon system given the constraints provided by lunar samples (Taylor 1975) and meteorites. The time of the Moon-forming impact is thought to have occurred as early as  $\sim 30$  Myr and as late as 110 Myr (Canup & Asphaug 2001; Canup 2004, 2008; Halliday 2008; Canup 2012; Ćuk & Stewart 2012), although the upper estimate remains relatively unconstrained by geochronology due to the wide range of ages for lunar rocks (Elkins-Tanton 2012). This timeline is applicable for the Solar System and, given that accretion is a chaotic process, is not expected to be the only model for other planetary systems around Sun-like stars.

In this article we explore the late stage accretion of terrestrial planets around a Sun-like star in a statistical manner in order to understand the types of collisions that lead to planet growth and the final giant impacts that bombard the planets that form. We can then compare the distributions of planet characteristics to those of the Solar System and estimate how common systems like our terrestrial planets may be around other stars in our galaxy.

## 3. NUMERICAL MODEL

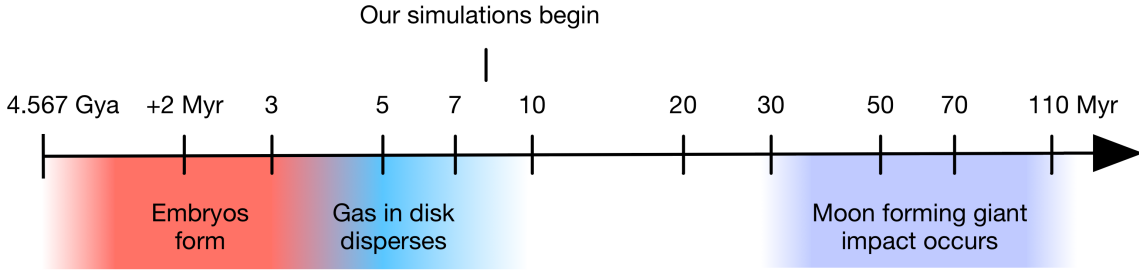


**Figure 1.** An approximate timeline for the formation of the Earth based on geochemical evidence and theoretical models. The oldest known chondrite meteorites date the beginning of Solar System formation to 4.567 billion years ago (Connelly et al. 2012). Within about 5 Myr, solid material in the protoplanetary disk accreted to form Mars-sized embryos embedded in a swarm of Moon-size and smaller planetesimals. Gas was still present up until about 3 – 7 Myr (Haisch et al. 2001; Hernandez et al. 2007, 2010) during which the cores of the giant planets accrete their gaseous envelopes (Lissauer 1987; Lissauer et al. 2009). Our simulations start at an epoch at which the gas in the disk has been dispersed and a disk of solid Moon-to-Mars-sized bodies remains. The so-called giant impact phase of planet formation starts some time after about 30 Myr, during which the Earth accretes the bulk of its mass. The Moon-forming giant impact also occurs some time after  $\sim 30$  Myr, but the timeline and impact scenario are still under debate.

The late stages of terrestrial planet formation – from embryos and planetesimals to planets – have been studied extensively with  $N$ -body algorithms that have greatly improved in both speed and functionality over the past few decades (Wetherill 1994, 1996; Chambers 1999, 2013; Levison & Duncan 2000). Early on, the primary goal of many of these studies was to broadly reproduce the masses and architecture of the four terrestrial planets in our Solar System. The wide diversity of newly discovered exoplanetary systems motivated the modification of these  $N$ -body models to address planet formation in different environments, such as in multiple-star systems (Chambers et al. 2002; Quintana et al. 2002, 2007; Quintana & Lissauer 2006), around stars of various stellar types (Lissauer 2007; Raymond et al. 2007), in the presence of inward migration of disk material (Mandell et al. 2007) and in the presence of various giant planet companions (Raymond et al. 2005; Raymond 2006; Quintana & Lissauer 2014). Models that included the accretion of water and volatile compounds to explore how Earth became a habitable planet soon followed (Raymond et al. 2004), as did higher resolution (a larger number of smaller bodies) simulations (Raymond 2006; O’Brien et al. 2006).

While a simple perfect-accretion model allows a broad study of the numbers and types of planets that can form under various circumstances, a model that allows fragmentation as an outcome of collisions is necessary to explore the history of collisions that lead to the formation of Earth-like planets and their affect on the final planet’s composition, dynamics and potential habitability. Leinhardt & Stewart (2012) developed a self-consistent set of scaling laws to map out the dynamical outcomes of gravity-dominated two-body collisions based on the masses, velocities and geometry of the bodies involved. Chambers (2013) implemented this collision mapping model into the  $N$ -body integration package *Mercury*, which we adopt for the simulations presented herein. The collision model is described next, followed by a description of the initial conditions of our simulations.

### 3.1. Collision model

For each collision event throughout an  $N$ -body simulation, the specific impact energy in the center of mass reference frame,  $Q$ , is computed by

$$Q = \frac{\mu v_{imp}^2}{2(m_{imp} + m_{tar})} \quad (1)$$

where  $m_{imp}$  is the mass of the impactor,  $m_{tar}$  is the mass of the target,  $\mu$  is the reduced mass, where

$$\mu = \frac{m_{imp} m_{tar}}{m_{imp} + m_{tar}}, \quad (2)$$

and  $v_{imp}$  is the impact velocity.

The collision model of Leinhardt & Stewart (2012) is essentially a set of scaling laws that predict the outcome of a collision by comparing  $Q$  with the criteria for catastrophic disruption between two colliding bodies,  $Q^*$ , which by definition is the specific impact energy needed to disrupt half of the total mass. The outcome can therefore be derived from the mass of the impactor ( $m_{imp}$ ), the target mass ( $m_{tar}$ ), the impact angle  $\theta$  (where  $\theta = 0$  degrees for a head-on collision) and the impact velocity  $v_{imp}$ . An input parameter to *Mercury* that affects the total number of bodies in a simulation is the minimum fragment mass,  $m_{frag}$ . If a collision leads to fragmentation, the mass of the largest remnant remaining from the target is recorded,  $m_{lr}$ , and the remaining mass from the target (or the impactor in some scenarios),  $m_{fragtot}$ , is broken up into  $x$  equal-sized fragments, where  $x = m_{fragtot} / m_{frag}$  (with any remainder mass less than  $m_{frag}$ ). The fragments are gravitationally dispersed at slightly above the escape velocity in uniform directions within a plane that includes the center-of-mass of the system. The evolution of these new fragments is then followed from that time forward while they gravitationally interact with other bodies in the disk. If a collision leads to net growth,  $m_{lr}$  is defined as the largest body formed from the mass of the target and impactor.

The outcome regimes of two-body collisions in our simulations with fragmentation include:

1. A collision with the central star (or outer giant planet) in which case the body is removed from the simulation
2. Ejection from the system if a body orbits beyond 100 AU from the central star
3. Perfect accretion (inelastic collisions) where the mass of the new body  $m_{lr}$  is equal to  $m_{imp} + m_{tar}$
4. A grazing collision that can lead to accretion or erosion. Grazing collisions occur when less than half of the projectile interacts with the target. In

this case the impact parameter  $b$  is greater than the critical impact parameter  $b_{crit} = r_{tar} / (r_{tar} + r_{imp})$ , where  $r_{tar}$  is the radius of the target and  $r_{imp}$  is the radius of the impactor

5. A non-grazing collision, where  $b < r_{tar}$ , that can lead to accretion or erosion
6. A ‘hit-and-run’ collision, discussed in detail in Asphaug et al. (2006); Genda et al. (2012), in which the target does not gain or lose a significant amount of mass, but the impactor may suffer fragmentation, so  $m_{lr} = m_{tar}$  and  $m_{fragtot} \leq m_{imp}$

At each collision event the initial and final masses, positions and velocities are recorded for the target, impactor and any fragments. In addition, parameters to characterize the collision are output such as the fate (type of collision), impact angle and impact velocity. All of the information needed to evaluate the collision history for planets that form in an  $N$ -body simulation is made available in the output of *Mercury*.

### 3.2. Initial conditions

Our simulations begin at the epoch of planet formation in which runaway and oligarchic growth have already taken place (Kokubo & Ida 1998) resulting in a bimodal disk mass distribution around the Sun. In total, 26 embryos and 260 planetesimals reside in our initial disk. The embryos are approximately Mars-sized ( $r_{em} = 0.56 R_{\oplus} \approx 3500$  km;  $m_{em} = 0.093 M_{\oplus}$ ) and are spread among approximately Moon-sized planetesimals ( $r_{em} = 0.26 R_{\oplus} \approx 1600$  km;  $m_{em} = 0.0093 M_{\oplus}$ ). All bodies are assumed to have a density of  $3 \text{ g cm}^{-3}$  to determine their radii and the bodies are placed between 0.35 AU to 4 AU from the Sun. The surface density of solids varies as  $a^{-3/2}$ , consistent with Solar Nebula models (Weidenschilling 1977), yielding a total disk mass of  $4.85 M_{\oplus}$ . The bodies begin on nearly circular and coplanar orbits with all other orbital elements (argument of periastron, longitude of ascending node and mean anomaly) selected at random. At the start of our simulations we include a Jupiter-mass planet at 5.2 AU and a Saturn-mass planet at 9.6 AU from the Sun at their present orbits and eccentricities and assume that these giant planets have already formed and that any gas in the disk has been dispersed. The problem is then purely gravitational and collisional, and any damping of the eccentricities and inclinations of embryos arises from dynamical friction from the swarm of smaller bodies and not by gas drag.

We implemented the same initial disk model as was used by Quintana & Lissauer (2014), in which several dozen simulations were performed with the perfect accretion model to examine the role of Jupiter and Saturn on water delivery to the terrestrial planets. This disk model was adapted from Chambers (2001) (which was also used by Chambers (2013) to test the fragmentation model), but we extrapolated our disk out from 0.35 to 4 AU whereas the disk in Chambers (2001, 2013) was truncated at 2 AU. The sizes of embryos and planetesimals remained the same in all studies, but there were only 14 embryos and 140 planetesimals in Chambers (2001) compared to our 26 embryos and 260 planetesimals.

Because  $N$ -body simulations are highly stochastic, we examine a large number of simulations in order to interpret our results statistically. We performed 280  $N$ -body simulations – 140 with fragmentation and 140 without – of accretion from the disk of bodies around a Sun-like star with Jupiter and Saturn analogs. The same set of elements for all bodies in the initial disk were used in each simulation apart from minuscule variations. Starting with the second simulation, we iteratively displaced a planetesimal near 1 AU by 1 meter along its orbit thereby creating a set of 140 initial disks that were all (slightly) different. In each simulation the evolution of all bodies in the disk was followed for 1 Gyr (note that in Section 5 we extended the fragmentation simulations to 2 Gyr).

An additional parameter that is needed for the integration is the minimum fragmentation mass which ultimately constrains the total number of bodies in a given simulation. We set the minimum fragmentation mass to be  $0.0047 M_{\oplus}$ , which is  $r_{frag} = 0.2 R_{\oplus} \approx 1300$  km, which is a little under half a lunar-mass. This is the same value used in Chambers (2013) and was adopted here for comparison. While smaller minimum fragmentation mass values would allow a better representation of the protoplanetary disk that formed our Solar System planets, this choice allowed us to perform a large number of simulations. The sensitivity of the results to this parameter are discussed in Section 5.3.

## 4. SIMULATION RESULTS

In this section we present the results from our 280 simulations of planet formation around the Sun with Jupiter and Saturn analogs perturbing the system from their current orbits. We ran 140 simulations of this system using the new fragmentation model and 140 simulations using our standard (perfect accretion) model in order to quantify the differences resulting from fragmentation.

Figure 2 shows the total number of bodies ( $1\text{-}\sigma$  ranges are shaded) from 140 simulations as a function of simulated time, with the standard simulations (without fragmentation) shown in red and those with fragmentation enabled shown in grey. All simulations began with the same 289 bodies: 26 Mars-sized embryos, 260 Moon-sized planetesimals, Jupiter, Saturn, and the Sun.

When fragmentation is enabled, the total number of bodies oscillates as the system undergoes accretion and fragmentation. Overall, the total number of bodies drops at a much slower rate compared to simulations that assume perfect accretion, as expected, and for the first few hundred million years there is a significant difference in the number of bodies at any given time among the two sets. With fragmentation, the number of bodies drops to half the initial number in 23 Myr whereas the perfect accretion simulations see the number of bodies fall to half the initial value in just 4 Myr – a factor of 6 difference. This leads to longer accretion timescales when fragmentation is included, although this divergence in accretion timescales is primarily due to the larger number of small bodies. The average time for the final planets to form (and for most of the small bodies to be accreted or ejected) with fragmentation is about 200–300 Myr, in contrast to the non-fragmentation simulations where accretion was complete by 100–200 Myr. Despite the different collision histories and timescales, the simulations ultimately converge towards a comparable final number



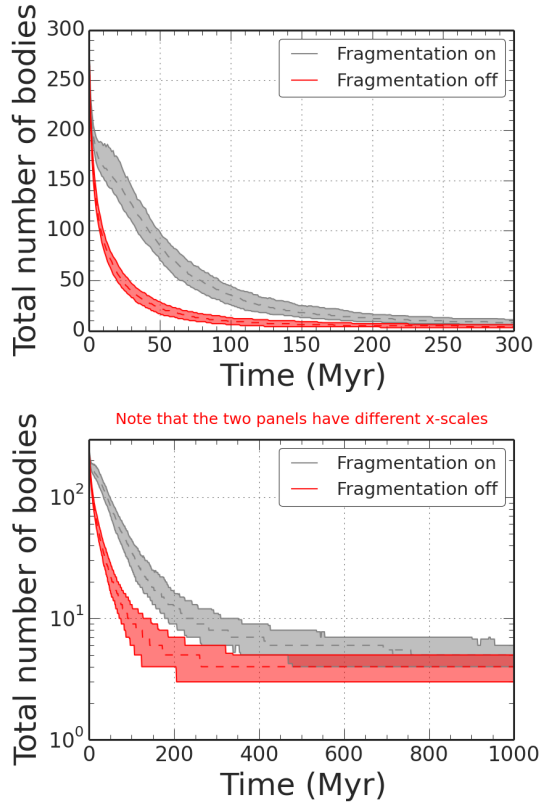
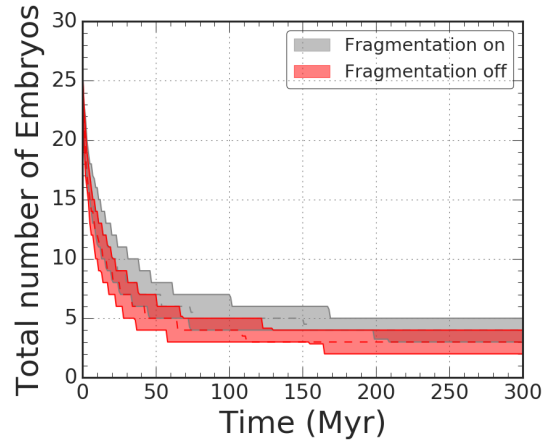


**Figure 2.** The total number of bodies remaining in our simulations as a function of time. The shaded regions show the 15th and 84th percentile which is equivalent to the  $1\text{-}\sigma$  bounds of the distribution. The red region shows the number of bodies in our simulations that utilize the standard *Mercury*  $N$ -body integrator while the grey region shows the results from simulations that include fragmentation. All simulations shown in this figure begin with 26 Mars-sized embryos embedded in a disk of 260 Moon-sized bodies and include Jupiter and Saturn analog planets. The upper and lower panels show the same data but with a linear and log vertical scale, respectively, to allow a better view of when the number of planets finalize. It should be noted that the horizontal scales of the two panels differ. Although both sets produce final planetary systems that are consistent, the collisional evolution is quite different among the two sets.

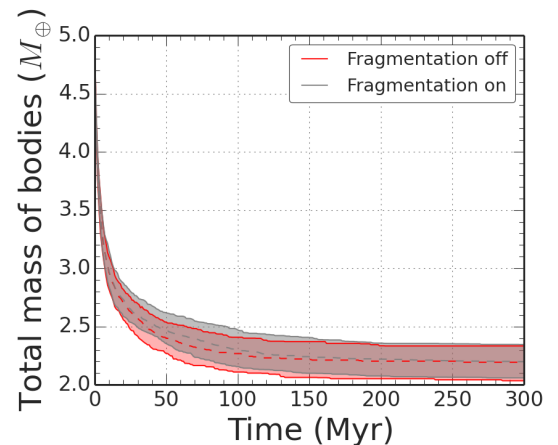
of planets (as shown in the lower panel of Figure 2 which shows the same data in log-space), in agreement with Chambers (2013).

Figure 3 compares just the number of embryos – which are the initial 26 Mars-sized bodies – as a function of simulation time. The number of embryos over time does not differ for the two different models as dramatically as the total number of bodies, thus the main difference among the two models shown in Figure 2 can be attributed to the planetesimals and fragments. On average  $3.9 \pm 0.9$  final planets formed in the simulations with fragmentation while  $3.0 \pm 0.8$  planets formed in the simulations with perfect accretion. In the 8 fragmentation runs performed in Chambers (2013), the average number of final planets was  $4.4 \pm 0.9$ , consistent with our findings. This demonstrates that despite the different formation histories of the planetary systems, fragmentation does not have a strong impact on the number of final planets.

The evolution of the average total mass remaining in the simulations is shown in Figure 4. During the first few hundred million years there is on average marginally



**Figure 3.** The total number of embryos remaining in our simulations as a function of time, where each initial disk begins with 26 Mars-sized embryos (as well as 260 planetesimals not included here). The symbols and colors are the same as those described in the caption of Figure 2. The number of embryos in the fragmentation model decreases at a slower rate than in the standard (perfect accretion) model, but not significantly so.



**Figure 4.** The median of the total mass remaining in the simulations as a function of time. The symbols and colors are the same as those described in the caption of Figure 2. Both models produce comparable results in terms of the total mass in the system remaining as a function of time. This is in contrast to the total number of bodies which decreases more slowly in the fragmentation model. This indicates that much of the material that is fragmented is re-accreted at later times rather than ejected from the system.

more mass available for collisions at a given time when fragmentation is included. By the time the final planets have formed, there is considerable overlap among the two sets of simulations. This is an indicator that a large fraction of the mass that is fragmented is ultimately re-accreted before it can escape the system.

The number of collisions as a function of simulation time is shown in Figure 5 and includes all collision events that occur in the 140 simulations with fragmentation enabled (shaded gray bars) and the 140 simulations that assumed perfect accretion (red shaded bars). Both the total number of collisions (top panel) and the percentage of total collisions (lower panel) are quite different among the two sets within the first 20 Myr. The total number of collisions is significantly higher when fragmentation is included, as expected. While there are 60% more collisions

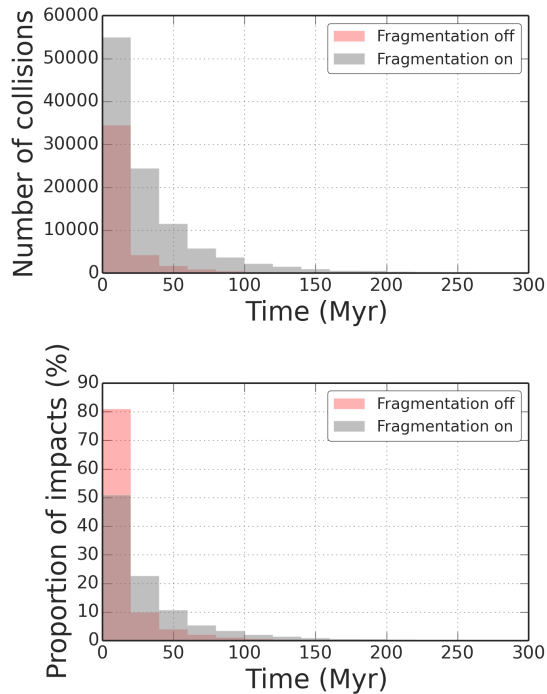


**Figure 5.** The number of impacts as a function of simulation time with fragmentation (gray) and without (red). The top panel shows the total number of impacts as a function of time for all our simulations while the lower panel shows the percentage of total impacts falling within that 20 Myr bin. While the total number of collisions is higher when fragmentation is included, only 50% of the collisions occur in the first 20 Myr, whereas 80% of the collisions occur in the first 20 Myr in the perfect accretion model. By 50 Myr, accretion is mostly complete when fragmentation is not included. Collisions in the fragmentation simulations continue for an additional 100 Myr. Despite these differences, the final planets that form in each set are comparable in terms of final mass and number.

within the first 20 Myr using the fragmentation model, these collisions only contribute to about 50% of the total number of collisions that occur in this model, whereas nearly 80% of the collisions in the standard model occur within the first 20 Myr. The time for the number of collisions to drop by a factor of two (the collisional half-life) for the perfect accretion simulations is 4 Myr compared with 19 Myr when fragmentation is included. The average time it takes for 90% of collisions to occur is 37 Myr for the perfect accretion simulations compared to 82 Myr for the fragmentation simulations, showing that the accretion timescales are approximately doubled when fragmentation is included.

In this section we have demonstrated that during the first 200 Myr or so the results from our fragmentation model differ significantly from the perfect accretion paradigm. In the next section we use this fragmentation model and focus on giant impacts onto Earth-like worlds to better understand the frequency and timescales of events that influence the final planet properties.

## 5. GIANT IMPACTS ONTO EARTH-ANALOGS

We now focus on Earth-like planets that form in simulations using our fragmentation model to evaluate characteristics of these planets that depend on their collision history. The Earth’s geological record has established that a large number of significant impacts onto

Earth helped to shape its composition and habitability. Small-scale examples include cratering events, some of which have caused mass extinctions (Lissauer & de Pater 2013). Larger-scale events include the Moon-forming impact and other giant impacts that have affected the Earth on a global scale. In our Solar System collisions ultimately led to the formation of four terrestrial planets and three moons within 2 AU of our Sun, with at least one of those planets remaining habitable despite the multitude of impacts.

It is unclear, however, if conditions in the Solar System were special for the Earth to form and retain an atmosphere and oceans. In theory, giant impacts can deliver or strip away water and other volatiles that are necessary ingredients for carbon-based life (Cameron 1983; Ahrens 1993; Lissauer & de Pater 2013). The timing of giant impacts is also important, because if a final giant impact occurs early enough in the planet’s accretion history, then sterilizing events can potentially be overcome by accretion of additional volatile-rich material that may still be available in the protoplanetary disk. If giant impacts occur late when most of the solid material in the disk has been accreted or ejected from the system, then the planet must rely on distant material like comets (which have a lower collision rate with bodies in the terrestrial region) for delivery of water and volatiles or else remain dry.

We extended the 1 Gyr fragmentation simulations presented in the previous section to 2 Gyr to examine the collisions that led to the formation of Earth-analogs. We define an Earth-analog as a final planet with a mass greater than  $0.5 M_{\oplus}$  that orbits with a semimajor axis between 0.75 and 1.5 AU from the Sun. Of the 140 simulations that included fragmentation, 96 simulations produced one Earth-analog, 34 produced two, and 1 run produced three Earth-analogs. Only 9 simulations resulted in zero Earth-analogs.

Figure 6 shows distributions of the number of final planets, the mass of the final planets, and the mass of the Earth-analogs that form in our fragmentation simulations. From 2 – 6 final planets form with masses ranging from that of Mars ( $\sim 0.1 M_{\oplus}$ ) to 1.6 times the mass of Earth. For the region where Earth now resides (0.75 – 1.5 AU), fewer low-mass planets form and the distribution is more centered around  $0.6 - 1 M_{\oplus}$ . We note that we also form analogs of Mars, Venus and Mercury, although our choice for the inner edge of the disk (0.35 AU) is not well suited to study the formation of Mercury-analogs.

### 5.1. Quantifying giant impacts

To examine the collisions experienced by the Earth-analogs formed in our models, we first need to determine how to quantify the impacts. Stewart et al. (2014) performed a suite of 3D hydrodynamic simulations of two-body gravitational collisions to study the types of collisions that could blow off a portion or all of an atmosphere or ocean, assuming the bodies involved had accreted an atmosphere and/or ocean. In their study, when the two bodies collide, the shock waves propagate and affect their atmospheres. Using a wide range of target and impactor masses, impact speeds, and impact angles, Stewart et al. (2014) found that variations in the shock pressure fields, and therefore the fraction of atmosphere loss, are highly sensitive to the impact parameter and mass ratio of the

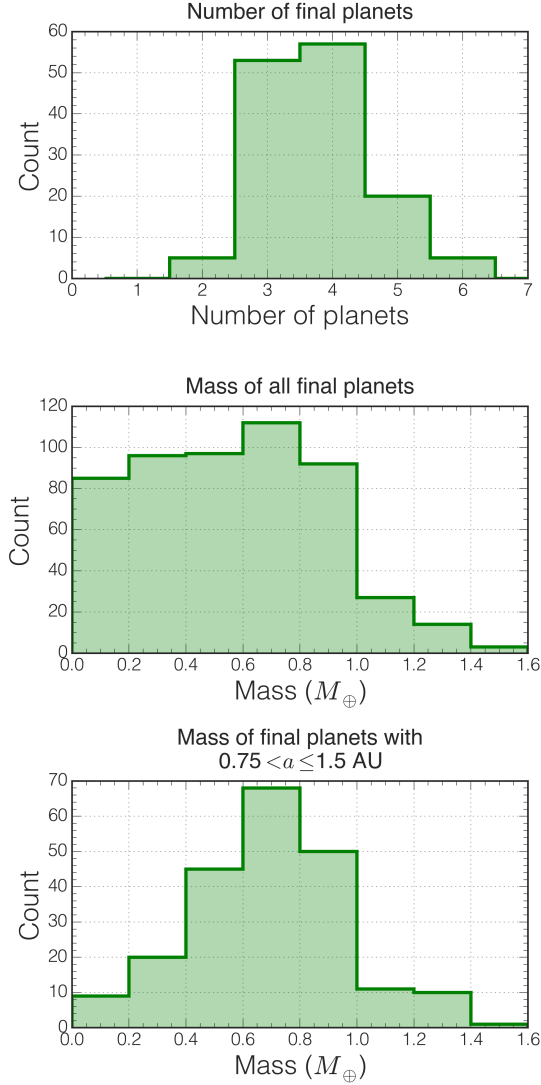


**Figure 6.** Histograms of the final planets formed in our simulations that included fragmentation. The top panel is the total number of final planets for all fragmentation simulations, where a planet is defined as a body with a mass larger than 0.9 Mars-mass. The middle panel shows the distribution of the masses of all final planets. The lower panel shows the mass distribution of final planets with final semi-major axes between 0.75 and 1.25 AU, which is the range in semimajor axis that defines an Earth-analog.

impactor to the target. Using the results from these hydrodynamic simulations, Lock et al. (2015) empirically derived a modified version of the specific impact energy  $Q$  (which is defined in Equation 1), designated  $Q_s$ , that better encapsulates variations in the shock pressure field and includes only the interacting mass of the two bodies:

$$Q_s = Q' \left( 1 + \frac{m_{imp}}{m_{tar}} \right) (1 - b) \quad (3)$$

At the point of contact, assuming the target is stationary, the impactor (the blue body in Figure 7) is traveling with impact velocity  $v_{imp}$  toward the target body (shown in brown). The impact parameter is defined as  $b = \sin\theta$  and the projected distance between the center of the two bodies at contact is  $B = (r_{imp} + r_{tar}) b$ , where  $r_{imp}$  and  $r_{tar}$  are the radii of the impactor and the target,

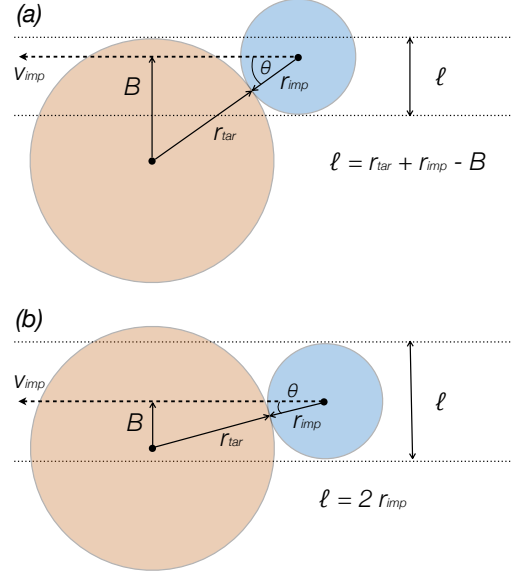


**Figure 7.** Geometry of a two-body collision. The parameter  $l$  is the projected length of the interacting mass and takes the value of  $r_{imp} + r_{tar} - B$  if the impact is grazing (panel a) and  $2r_{imp}$  if the impactor fully interacts with the target (panel b).

respectively. The projected length of the impactor that intersects the target is  $l$  and, depending on whether the impactor fully interacts with the target, can take a value of

$$l = \begin{cases} 2 r_{imp} & \text{if } B + r_{imp} \leq r_{tar} \\ r_{imp} + r_{tar} - B & \text{if } B + r_{imp} > r_{tar}. \end{cases} \quad (4)$$

These two cases are shown in the upper and lower panels of Figure 7.

The specific impact energy,  $Q_s$ , is a function of the ratio of the impactor mass ( $m_{imp}$ ) to the mass of the target ( $m_{tar}$ ), the impact parameter  $b$ , and  $Q'$  which is a modified version of  $Q$  that takes into account only the interacting mass of the two bodies. As shown in Lock et al. (2015),  $Q'$  can be calculated by scaling  $Q$  by the ratio of the reduced mass for the interacting mass,  $\mu_\alpha$ , to the reduced mass  $\mu$  as defined in Equation 2

$$Q' = \frac{\mu_\alpha}{\mu} Q \quad (5)$$

The interacting reduced mass is

$$\mu_\alpha = \frac{\alpha m_{imp} m_{tar}}{\alpha m_{imp} + m_{tar}} \quad (6)$$

where  $\alpha$  is the fraction of the impactor mass that interacts and is defined as

$$\alpha = \frac{3 r_{imp} l^2 - l^3}{4 r_{imp}^3} \quad (7)$$

The original and full derivation of these impact geometries are given in Leinhardt & Stewart (2012) and Lock et al. (2015).

To associate  $Q_s$  to physical events on planets, Stewart et al. (2014) showed that, for an atmosphere-to-ocean ratio of 1:300, an impact with  $Q_s > 10^7$  J/kg was needed to strip 100% of an atmosphere, and an order of magnitude

greater energy ( $Q_s > 10^8$  J/kg) was needed to remove an entire ocean. By evaluating the values of  $Q_s$  for collisions involved in a previous numerical  $N$ -body study of late stage planet formation (Raymond et al. 2009), one which assumed perfect accretion, Stewart et al. (2014) found that impacts that could cause partial atmospheric loss were common but impacts with energies sufficient to blow off an entire atmosphere or ocean were rare. Herein, we adopt  $Q_s$  as our parameter of interest to evaluate the collisions in our fragmentation simulations, particularly those that lead to the formation of an Earth-analog.

The Moon-forming giant impact, which was likely the final significant giant impact during the Earth’s formation, can also be parameterized in terms of  $Q_s$  (Lock et al. 2015). Leading theories for the formation of the Moon suggest that a giant collision occurred between the proto-Earth and another object, resulting in a remnant disk from which the Earth’s Moon formed (Canup & Asphaug 2001; Canup 2004, 2008, 2012; Ćuk & Stewart 2012). Based on estimates of the age of the lunar melt, this collision likely occurred some time between 30 – 110 Myr after the Solar System began to form (Taylor 1975; Halliday 2008), however it could have occurred later (see Section 2). The characteristics and orbits of the bodies involved in these models, however, remain unclear since there are several scenarios that can form the Moon while satisfying observational constraints (the angular momentum of the Earth-Moon system) and isotopic compositional constraints provided by lunar samples. By using  $Q_s$  to quantify both the Moon-forming impact and the giant impacts in our simulations, we can draw comparisons without having to adopt a specific Moon-formation model (impact geometry and impactor mass). Note that many impacts comparable to the Moon-forming impact may not have enough angular momentum to produce a Moon-forming disk. The full range of  $Q_s$  for the canonical Moon-forming impact is  $0.3 \times 10^6 - 2 \times 10^6$  J/kg (Canup & Asphaug 2001; Canup 2004). For models that require higher angular momenta (Canup 2012; Ćuk & Stewart 2012), the range of  $Q_s$  is about  $2 \times 10^6 - 2.5 \times 10^7$  J/kg (Stewart et al. 2014).

Because the values of  $Q_s$  span a wide range for the various Moon-formation models, we chose to define a ‘giant impact’ threshold value for the collisions in our simulations at  $Q_s \geq 2 \times 10^6$  J/kg (equivalent to  $\log_{10} Q_s = 6.3$ ). This corresponds to the minimum impact energy from the more recent high angular momentum Moon-forming impact models (Canup 2012; Ćuk & Stewart 2012). Significant ( $\gtrsim 50\%$ ) atmosphere stripping also begins with specific impact energies at this threshold, so this choice allows us to define a giant impact as one comparable to the Moon-forming impact and one that could potentially annihilate any life that may have evolved (Sleep et al. 1989) due to the effects on the planet’s atmosphere and surface.

We computed  $Q_s$  for all impacts that were involved in the formation of an Earth-analog for all of our fragmentation simulations. As illustrated in Figure 8, impacts with enough energy to strip entire atmospheres ( $Q_s \geq 10^7$  J/kg) and oceans ( $Q_s \geq 10^8$  J/kg) are rare, a result consistent with those of Stewart et al. (2014). The percentage of impacts with Moon-forming energies is just 5% of all impacts, while less than 0.2% of impacts are energetic

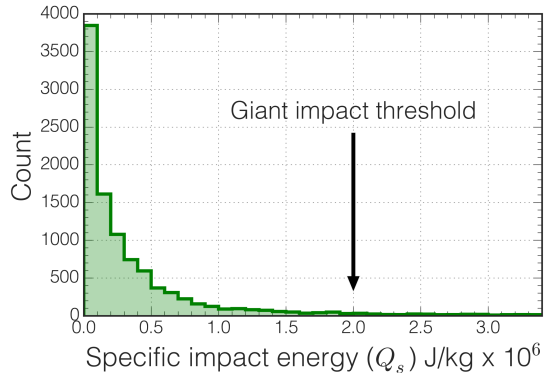


**Figure 8.** The specific impact energy  $Q_s$  for all impacts onto Earth-analog planets. Here we show the energies in linear space to demonstrate that the vast majority of impacts are low energy. Our giant impact threshold is set at  $2 \times 10^6$  J/Kg. Just 5% of impacts have energies above our giant impact threshold. Most giant impacts are head-on smashes.

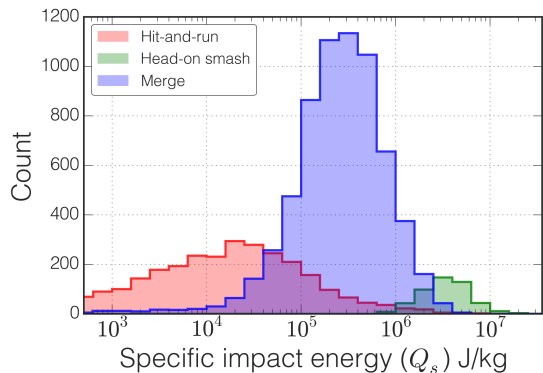


**Figure 9.** Specific impact energies,  $Q_s$ , for all impact events that led to the formation of an Earth-analog grouped into three types of impacts. An Earth-analog is defined as a planet with mass  $> 0.5 M_{\oplus}$  that orbits within 0.75 – 1.5 AU from the Sun. Hit-and-run impacts (shaded red) account for 31% of the impacts that produced Earth-analogs, head-on impacts (shaded green) account for 5%, and all collisions that led to mergers (shaded blue) account for 64% of the collisions. We are interested in values of  $Q_s$  that reach or exceed  $2 \times 10^6$  J/kg, a specific impact energy consistent with the Moon-forming impact event according to recent models. Impact energies above this threshold are also sufficient to strip over half of a planet’s atmosphere.

enough to fully strip an atmosphere of an Earth-analog planet.

Figure 9 shows the distribution of these energy values grouped according to three types of impacts: merging events (grazing and non-grazing events that led to net growth), hit-and-run events, and head-on collisions. The majority (64%) of events result in a merger while 31% are hit-and-run collisions. The remaining 5% of impacts are head-on collisions with high values of  $Q_s$ . While head-on collision events are uncommon, they account for all events that are capable of stripping a planet of its atmosphere. For collisions that led to the formation of Earth-analogs in the eight fragmentation runs performed by Chambers (2013), 70% resulted in net growth, 30% were hit-and-run events, and zero collisions led to net erosion. Our results are consistent, considering the relatively small number of simulations and the less massive initial disk used in Chambers (2013).



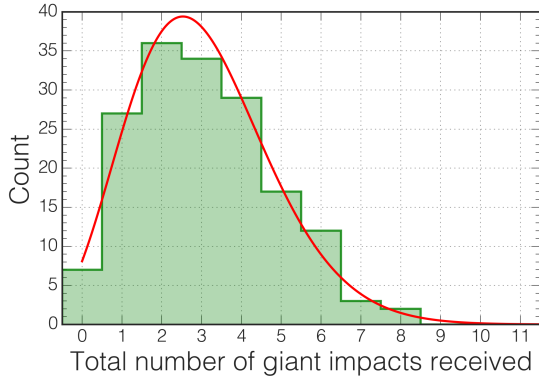


**Figure 10.** A histogram showing the total number of giant impacts received per Earth-analog in all of the 2 Gyr fragmentation simulations. We define a giant impact as an impact where  $Q_s > 2 \times 10^6 \text{ J kg}^{-1}$ . The red curve shows a Poisson probability mass function fit to the data. The mean number of giant impacts per Earth-analog is 3.0 but the number of giant impacts received ranges from 1 – 8.

We next computed the total number of giant impacts experienced by each Earth-analog during their formation. A histogram of these results is shown in Figure 10, where the bins with the highest occurrence is at two and three giant impacts. Owing to this being a discrete distribution with a number of events occurring within a fixed time window, we are able to describe the resulting probability mass function as a Poisson distribution. We fit these data of the number of giant impacts and found best fitting parameters of  $\lambda = 3.04$ , which yields the red curve shown in Figure 10. This Poisson distribution function has a mean at 3.0 and a median of 3.4. While each of these giant impacts is likely to deplete the volatile content of the planet (c.f. Stewart et al. 2014), most of these giant impacts are unlikely to fully strip an atmosphere and ocean.

### 5.2. Final giant impact time

The *final* giant impact received by an Earth-analog largely influences its dynamical state and bulk composition. With the relatively large number of simulations performed in this work, we can make probabilistic inferences from the distributions of the collision times and characteristics of the final giant impacts onto Earth-analogs.

In Figure 11 we show the distribution of times of the final giant impact onto an Earth-analog in all of our fragmentation simulations. All but seven of our Earth-analog planets experience at least one giant impact during their evolution. About 56% experience their last giant impact within the first 50 Myr of the simulation and 75% experience their final giant impact within the first 100 Myr. This mirrors our understanding of the range of feasible times for the Earth’s Moon-forming impact (Figure 1). In terms of final giant impact times, we find that the Earth (assuming the Moon-forming impact was its final giant impact) is relatively typical.

The time of the final giant impact onto an Earth-analog is likely correlated with the late (post-impact) mass accreted by that Earth-analog, primarily because the abundance of solid material available to accrete likely decreases with time. This has implications for a planet’s habitability. If an Earth-analog is stripped of volatiles

late in its formation, for example, there may not be enough volatile-rich material remaining in the disk for that planet to accrete. Jacobson et al. (2014) illustrated this correlation using a large set of  $N$ -body (perfect-accretion) simulations. For simulations that included giant planets near their current orbits (comparable to our simulations), they found the fraction of mass accreted by an Earth-analog after its final giant impact ranged from about 10 – 20% for impacts occurring at 10 Myr to about 1% for final impacts at around 100 Myr. In Figure 12 we show, for all of our fragmentation simulations, a similar correlation between the final giant impact time for an Earth-analog and the fraction of mass the planet accreted after the impact. Compared to Jacobson et al. (2014), our results are biased towards higher fractions of late mass accreted for a given final giant impact time. This is not surprising, given the differences in the initial conditions and definitions used in each study. First, our definition for a giant impact relies on a minimum specific impact energy that is physically motivated and more stringent, whereas Jacobson et al. (2014) define a giant impact as a collision between an Earth-analog and a surviving Moon-size or Mars-size embryo (comparable to our initial planetesimals and embryos). Second, the initial disks used in Jacobson et al. (2014) began with half of the disk mass in about 100 bodies that are Moon-size to Mars-size and half of the disk in thousands of non-mutually interacting Ceres-sized (about 470 km) planetesimals. Our disk begins with half of the mass in 26 Mars-size embryos and the other half in 260 Moon-size planetesimals, and fragments are allowed during the simulation with a minimum resolution of about half a Moon mass. A direct comparison is therefore difficult, especially given that Jacobson et al. (2014) found the mean time of the final giant impact was sensitive to the mass ratios of the bodies in the disk.

The fraction of mass that Earth accreted after the Moon-forming impact has been inferred to be less than 1% from the abundance of highly siderophile elements in the Earth’s mantle compared to abundances found in chondritic meteorites (Jacobson et al. 2014). Using an estimate of the Earth’s late accreted mass of  $0.003 - 0.006 M_{\oplus}$ , combined with the numerically-derived relation between late accreted mass and final giant impact, Jacobson et al. (2014) placed constraints on the time of the Moon-forming impact to  $95 \pm 32$  Myr after the start of the Solar System. This estimate was based on simulations that included giant planet migration. For their classical simulations (which are comparable to ours in terms of the orbits of the giant planets), the median time of the Moon-forming impact increases to about 110 Myr. Although our results are not complete at the lower end of late accreted mass estimates due to our initial resolution, our results are consistent with the estimates based on the classical simulations of Jacobson et al. (2014).

Our motivation in this work is not to model and constrain the timing of the Earth’s Moon-forming impact, but to examine in a statistical manner the frequency and timescales of giant impacts analogous to the Moon-forming impact onto Earth-like planets that form around Sun-like stars. The distribution of mass ratios and impact velocities of the final giant impacts in our simulations, however, may shed some light on the likelihood of a given scenario that may be useful for comparing Moon-

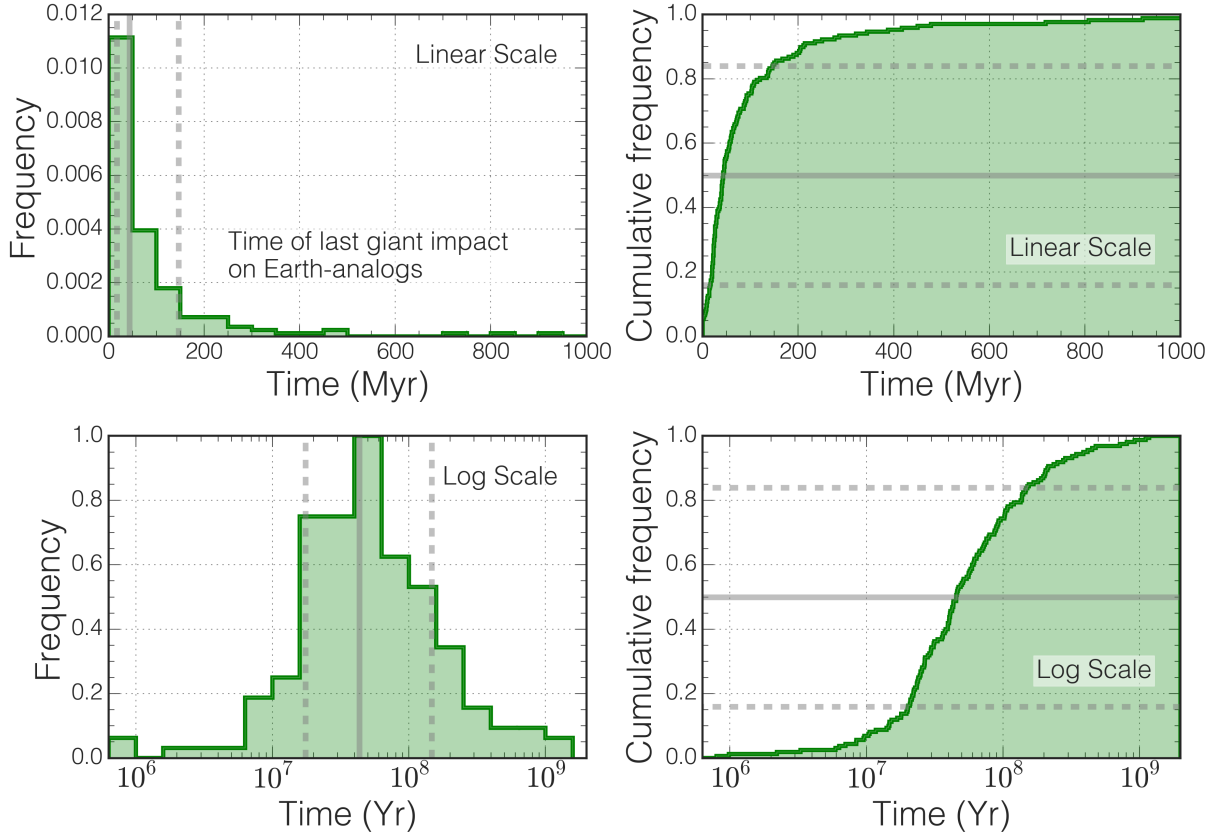


**Figure 11.** The distribution of times of last giant impact (defined by  $Q_s > 2 \times 10^6 \text{ J kg}^{-1}$ ) for Earth-analogs that survive the duration of the simulation. The left panels show a histogram of the time of last giant impact with bin-width of 50 Myr. The right panels show the cumulative frequency of the same distribution. The gray dashed lines are drawn at the 15.9 and 84.1 percentiles and the gray solid lines are drawn at the median of the distribution. The 15.9, 50 and 84.1 percentiles are at 17 Myr, 43 Myr and 147 Myr after the beginning of the simulations, respectively. The upper panels show the data in linear space and the lower panels in log space.

formation models. In Figure 13 we show the ratio of the impactor mass to the target mass as a function of the impact velocity (scaled by the escape velocity) for all final giant impacts onto the Earth-analogs that formed in our fragmentation simulations. Most impact events that involve bodies of comparable mass have impact velocities that are 1 – 1.5 times the escape velocity, whereas smaller relative impactors reach impact velocities up to 5 times the escape velocity.

The time of the final giant impact plays a large role on a planet’s potential habitability. The emergence of life on Earth, and whether there were multiple origins due to life-sterilizing giant impacts, remains unclear despite the multitude of long-standing theories. Nonetheless, the oldest known microfossils date the development of life to roughly 1 Gyr after the Solar System formed (Awramik 1992) and there is indirect evidence for life occurring even earlier (Mojzsis et al. 1996; McKeegan et al. 2007; Bella et al. 2015). In our fragmentation simulations, which were extended to 2 Gyr, 20-30% of planetary systems experience a giant impact after planet formation has essentially finished (100 – 200 Myr into the simulation). Only 2 of our 167 Earth-analogs experience a giant impact after 1 Gyr. Higher resolution simulations can provide better constraints on the distribution of late life-sterilizing impacts, as objects smaller than those simulated here can also be detrimental to any life that may have formed. Our simulations show that giant impacts

that are capable of stripping half of an atmosphere (and are therefore likely detrimental to life on a global scale) may not pose a substantial threat for Earth-like planets that form around Sun-like stars if the timescales for the appearance of life on Earth are typical.

### 5.3. On the validity of the initial conditions

Here we briefly address some caveats that should be considered when interpreting these (and other similar  $N$ -body) results. Firstly, our initial conditions begin with objects that are roughly Moon-sized to Mars-sized. In reality the initial disk would contain these in addition to a significantly larger number of small bodies. In most  $N$ -body accretion simulations a much higher fidelity is usually desired but must be balanced with available computational resources.

The choice of the minimum fragmentation mass in our model constrains the total number of objects. We selected a minimum fragmentation mass of a little under 0.5 a lunar-mass, the same value used in Chambers (2013), so we could compare results and also perform a statistically large sample of simulations in a reasonable time. It is expected that the final planets that form, and their collision histories, will be different with the selection of a less massive (and more physically justified) minimum fragmentation mass.

Of particular concern in this work was whether our conclusions on the numbers and times of giant impacts

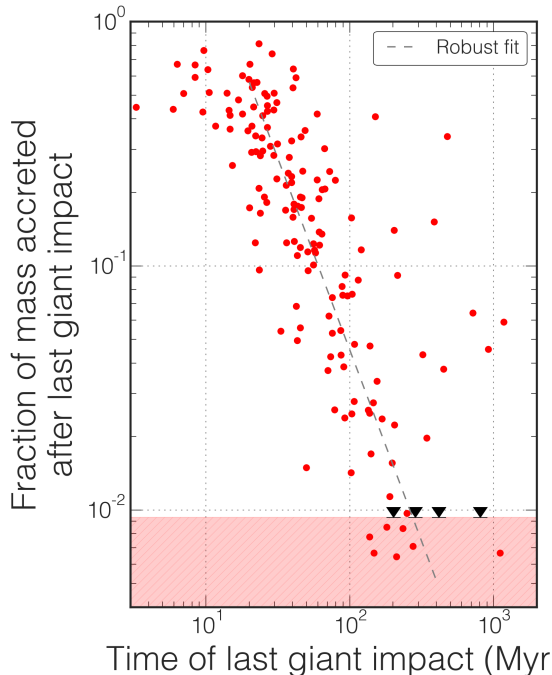


**Figure 12.** The proportion of material that was accreted by an Earth-analog after its last giant impact, plotted against the time of that last giant impact, is shown for all of the Earth-analogs that formed in our fragmentation simulations. More mass is accreted if the final impact occurs early (following Jacobson et al. 2014). The red hatched region shows where we have poor sensitivity because it is smaller than our initial minimum planetesimal mass of  $0.009 M_{\oplus}$ . The black upper limit points show bodies where no additional material was accreted after the final giant impact. If our minimum fragment size were smaller these planets would likely have accreted lower mass material at late times. The gray line is a robust fit to the red data with giant impacts after 20 Myr.

are biased by our minimum fragment mass. In Figure 14 we show the specific impact energies of all impacts onto Earth-analogs split into two populations, (a) impactors more massive than one lunar mass and (b) impactors less massive than one lunar mass, where one lunar mass is approximately equal to the initial mass of the planetesimals in our simulations. We found that while only a third of total impactors have a mass of at least one lunar mass, 93% of giant impacts are from bodies at least as large as our initial planetesimal mass. Therefore, our results are unlikely to depend strongly on the initial fragment mass since very few of the giant impact are from fragments - in other words, lowering the minimum fragment mass would only effect no more than 7% of our giant impacts.

## 6. SUMMARY AND CONCLUSIONS

We have presented a large set of numerical simulations of late stage terrestrial planet formation around a Sun-like star with outer planets analogous to Jupiter and Saturn perturbing the system. In total, 280  $N$ -body simulations were performed, which is an order-of-magnitude larger number than nearly all previous numerical studies of this stage have each presented. Half of the simulations used a standard perfect-accretion model, in which all collisions lead to mergers. The other half used an  $N$ -body algorithm that has recently been modified to include a state-of-the-art collision model (Chambers 2013), allowing a wider range of collision outcomes including

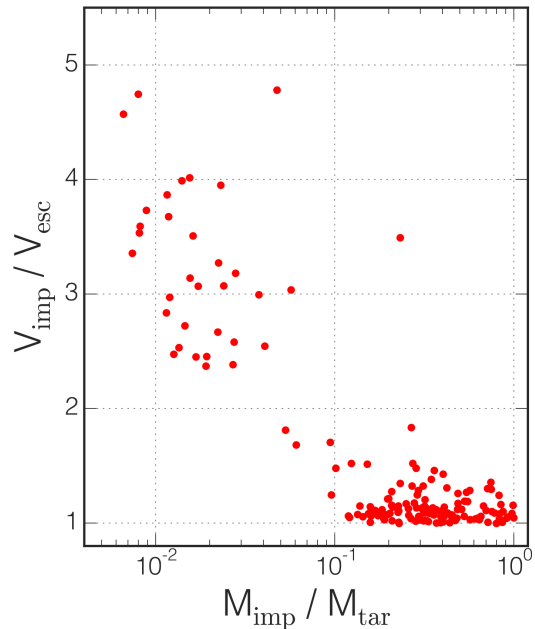


**Figure 13.** For each final giant impact onto every Earth-analog we show the velocity of that impact relative to the escape velocity of the planets as a function of the mass ratio of the impacting body to the final planet. Smaller bodies have a higher relative impact velocity than larger impacting bodies. Collisions where the impactor is an embryo mass body typically occur as just above the escape velocity.

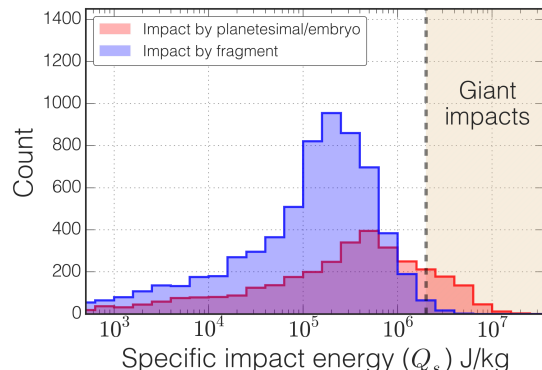


**Figure 14.** Specific impact energies,  $Q_s$ , for all impactors onto the Earth-analogs that formed in our fragmentation simulations. The blue-shaded region represents material that had been previously fragmented, and the red-shaded region represents material that was at least as massive as our initial planetesimals (about the mass of the Moon). 93% of the impactors that were involved in giant impacts (according to our definition as given in Figure 11) were by bodies that were non-fragments. Therefore, our minimum fragment size does not have a significant effect on our statistics of giant impacts.

fragmentation and hit-and-run impacts. All simulations began with virtually the same initial disk of hundreds of Moon to Mars-sized bodies and were evolved forward in time for 1 Gyr.

We found that when fragmentation is enabled, the number of final planets and their mass distribution were consistent with those formed in the standard model, however the collision history of these planets differed significantly among the two sets. The typical accretion timescale (measured by the total number of bodies re-

maining in the system) were approximately doubled in the fragmentation simulations. The number of larger embryos and the total mass remaining as a function of time, however, were comparable in both models suggesting that much of the fragmented material was eventually re-accreted. In our fragmentation simulations, only about 64% of all collisions lead to merging (and most of these mergers resulted in some fragmentation), validating the importance of including fragmentation when studying characteristics of terrestrial planet formation that depend on the collision history. We advise that caution should be used when inferring results based on the collisional history of planet, such as composition and habitability, from  $N$ -body planet formation models that assume perfect accretion.

We next focused on our fragmentation simulations, which were extended to 2 Gyr, to examine the collision history of the Earth-analogs that formed. We defined an Earth-analog as a planet that formed between 0.75 – 1.5 AU from the Sun and had a mass  $> 0.5 M_{\oplus}$ . Of the 140 simulations that included fragmentation, 131 produced at least one Earth-analog and 35 produced two or more.

To quantify the impacts onto the Earth-analogs, we adopted a unit of specific impact energy  $Q_s$  developed by Lock et al. (2015) which takes into account the mass ratio and impact geometry of a two-body collision. We computed  $Q_s$  for all impacts onto the Earth-analogs that formed in our fragmentation simulations. We then defined a threshold for a ‘giant impact’ of  $Q_s = 2 \times 10^6$  J/kg, which is the minimum  $Q_s$  value for some recent (high-angular momentum) Moon-formation scenarios and is also a value energetic enough to strip around half of an Earth-like planet’s atmosphere.

All but seven of the Earth-analogs experienced at least one giant impact, according to our definition, and the average number of such impacts was 3.0 per planet within the 2 Gyr simulations. Just 15 of the 167 Earth-analogs in our simulations received an impact with an energy above  $10^7$  J/kg – our full atmosphere stripping criterion, and no Earth-analog experienced an impact capable of stripping an entire ocean. These results show that very high impact events are exceptionally uncommon and that most planets do not even experience an impact that would leave the planet completely atmosphere free.

The *final* giant impact onto an Earth-like planet has implications for its composition and volatile inventory. If a final giant impact occurs early enough, there may still be volatile-rich material in the disk available for Earth-analogs to accrete. In the first 50 Myr, 56% of the Earth-analogs experienced their final giant impact, and 75% had their final impact within 100 Myr. The median final giant impact time for all Earth-analogs in our fragmentation simulations was 43 Myr with  $\pm 1\sigma$  equivalent intervals at 17 and 147 Myr, consistent with leading Moon-formation models developed for the Solar System. Just two of our Earth-analogs experienced a giant impact between 1 Gyr (the time at which we have fossil evidence of life on earth) and 2 Gyr (when we ended our simulations) after the beginning of the simulation. This is suggestive that relatively few Earth-analogs that develop life on timescales comparable to Earth are later dealt a fatal blow by a late giant impact.

The initial conditions of the giant planets should be taken into consideration when interpreting the results

presented herein. Classical models of the Solar System have assumed that the giant planets formed in situ (Chambers 2001, 2013; Quintana & Lissauer 2014). All of our simulations presented herein have adopted this model and include analogs to Jupiter and Saturn near their present orbits. Recent models have suggested that the giant planets may have originated on more eccentric orbits or may have undergone significant migration (Raymond et al. 2009; Walsh et al. 2012; Raymond & Morbidelli 2014). Because these giant planets are the largest perturbers (not counting the central star), their configuration can significantly alter the growth of the terrestrial planets. For this article we chose to limit the parameter space to one configuration, Jupiter and Saturn at their present orbits, in order to perform a large number of simulations with comparable initial conditions. Exploring the effects of various giant planet configurations on the collision history of Earth-analogs would benefit Solar System models as well as planetary systems formed around other Sun-like stars in our galaxy.

The authors would like to thank Jack Lissauer, Billy Quarles, Chris Henze, Simon Lock and Sarah Stewart for comments that improved this manuscript. E.V.Q is supported by a NASA Senior Fellowship at the Ames Research Center, administered by Oak Ridge Associated Universities through a contract with NASA. The simulations presented here were performed using the Pleiades Supercomputer provided by the NASA High-End Computing (HEC) Program through the NASA Advanced Supercomputing (NAS) Division at Ames Research Center.

## REFERENCES

- Ahrens, T. J. 1993, *Annual Review of Earth and Planetary Sciences*, 21, 525
- Asphaug, E., Agnor, C. B., & Williams, Q. 2006, *Nature*, 439, 155
- Awramik, S. M. 1992, *Photosynth Res.*, 33, 75
- Bella, E. A., Boehnke, P., Harrison, T. M., & Mao, W. L. 2015, *Proceedings of the National Academy of Sciences*, TDB
- Bonsor, A., Leinhardt, Z. M., Carter, P. J., et al. 2015, *Icarus*, 247, 291
- Cameron, A. G. W. 1983, *Icarus*, 56, 195
- Canup, R. M. 2004, *Icarus*, 168, 433
- . 2008, *Icarus*, 196, 518
- . 2012, *Science*, 338, 1052
- Canup, R. M., & Asphaug, E. 2001, *Nature*, 412, 708
- Chambers, J. E. 1999, *MNRAS*, 304, 793
- . 2001, *Icarus*, 152, 205
- . 2013, *Icarus*, 224, 43
- Chambers, J. E., Quintana, E. V., Duncan, M. J., & Lissauer, J. J. 2002, *AJ*, 123, 2884
- Connolly, J. N., Bizzarro, M., Krot, A. N., et al. 2012, *Science*, 338, 651
- Ćuk, M., & Stewart, S. T. 2012, *Science*, 338, 1047
- Dauphas, N., & Pourmand, A. 2011, *Nature*, 473, 489
- Elkins-Tanton, L. T. 2012, *Annual Review of Earth and Planetary Sciences*, 40, 113
- Fischer, R. A., & Ciesla, F. J. 2014, *Earth and Planetary Science Letters*, 392, 28
- Genda, H., Kokubo, E., & Ida, S. 2012, *ApJ*, 744, 137
- Goldreich, P., & Ward, W. R. 1973, *ApJ*, 183, 1051
- Haisch, Jr., K. E., Lada, E. A., & Lada, C. J. 2001, *ApJ*, 553, L153
- Halliday, A. N. 2008, *Royal Society of London Philosophical Transactions Series A*, 366, 4163
- Hernandez, J., Morales-Calderon, M., Calvet, N., et al. 2010, *ApJ*, 722, 1226



- Hernandez, J., Hartmann, L., Megeath, T., et al. 2007, *ApJ*, 662, 1067
- Jacobson, S. A., Morbidelli, A., Raymond, S. N., et al. 2014, *Nature*, 508, 84
- Kokubo, E., & Ida, S. 1998, *Icarus*, 131, 171
- . 2000, *Icarus*, 143, 15
- Krijt, S., Ormel, C. W., Dominik, C., & Tielens, A. G. G. M. 2015, *A&A*, 574, A83
- Leinhardt, Z. M., & Stewart, S. T. 2012, *ApJ*, 745, 79
- Levison, H. F., & Duncan, M. J. 2000, *AJ*, 120, 2117
- Lines, S., Leinhardt, Z. M., Paardekooper, S., Baruteau, C., & Thebault, P. 2014, *ApJ*, 782, L11
- Lissauer, J. J. 1987, *Icarus*, 69, 249
- . 1993, *ARA&A*, 31, 129
- . 2007, *ApJ*, 660, L149
- Lissauer, J. J., & de Pater, I. 2013, *Fundamental Planetary Science*, Cambridge University Press
- Lissauer, J. J., Hubickyj, O., D'Angelo, G., & Bodenheimer, P. 2009, *Icarus*, 199, 338
- Lock, S., et al. 2015, *TBD*, 1, 1
- MacPherson, G. J. 2014, *Calcium-Aluminum-Rich Inclusions in Chondritic Meteorites*, ed. A. Balogh, A. Bykov, P. Cargill, R. Dendy, T. Dudok de Wit, & J. Raymond, 139–179
- Mandell, A. M., Raymond, S. N., & Sigurdsson, S. 2007, *ApJ*, 660, 823
- McKeegan, K. D., Kudryavtsev, A. B., & Schopf, J. W. 2007, *Geology*, 35, 591
- Mojzsis, S. J., Arrhenius, G., McKeegan, K. D., et al. 1996, *Nature*, 384, 55
- Morbidelli, A., Lunine, J. I., O'Brien, D. P., Raymond, S. N., & Walsh, K. J. 2012, *Annual Review of Earth and Planetary Sciences*, 40, 251
- O'Brien, D. P., Morbidelli, A., & Levison, H. F. 2006, *Icarus*, 184, 39
- Quintana, E. V., Adams, F. C., Lissauer, J. J., & Chambers, J. E. 2007, *ApJ*, 660, 807
- Quintana, E. V., & Lissauer, J. J. 2006, *Icarus*, 185, 1
- Quintana, E. V., & Lissauer, J. J. 2010, in *Astrophysics and Space Science Library*, Vol. 366, *Astrophysics and Space Science Library*, ed. N. Haghighipour, 265
- . 2014, *ApJ*, 786, 33
- Quintana, E. V., Lissauer, J. J., Chambers, J. E., & Duncan, M. J. 2002, *ApJ*, 576, 982
- Raymond, S. N. 2006, *ApJ*, 643, L131
- Raymond, S. N., & Morbidelli, A. 2014, *ArXiv e-prints*
- Raymond, S. N., O'Brien, D. P., Morbidelli, A., & Kaib, N. A. 2009, *Icarus*, 203, 644
- Raymond, S. N., Quinn, T., & Lunine, J. I. 2004, *Icarus*, 168, 1
- . 2005, *Icarus*, 177, 256
- . 2006, *Icarus*, 183, 265
- Raymond, S. N., Scalo, J., & Meadows, V. S. 2007, *ApJ*, 669, 606
- Safronov, V. S., & Zvjagina, E. V. 1969, *Icarus*, 10, 109
- Sleep, N. H., Zahnle, K. J., Kasting, J. F., & Morowitz, H. J. 1989, *Nature*, 342, 139
- Stewart, S. T., & Leinhardt, Z. M. 2012, *ApJ*, 751, 32
- Stewart, S. T., Lock, S. J., & Mukhopadhyay, S. 2014, in *Lunar and Planetary Inst. Technical Report*, Vol. 45, *Lunar and Planetary Science Conference*, 2869
- Tang, H., & Dauphas, N. 2014, *Earth and Planetary Science Letters*, 390, 264
- Taylor, S. R. 1975, *Lunar science - a post-Apollo view. Scientific results and insights from the lunar samples.*
- Walsh, K. J., Morbidelli, A., Raymond, S. N., O'Brien, D. P., & Mandell, A. M. 2012, *Meteoritics and Planetary Science*, 47, 1941
- Weidenschilling, S. J. 1977, *Ap&SS*, 51, 153
- Wetherill, G. W. 1994, *Geochim. Cosmochim. Acta*, 58, 4513
- . 1996, *Icarus*, 119, 219